A theoretical study of the reverse water-gas shift reaction on Ni(111) and Ni(311) surfaces

Received: 11 July 2019 | Accepted: 2 August 2019

DOI: 10.1002/cjce.23655

ARTICLE

THE CANADIAN JOURNAL OF CHEMICAL ENGINEERING

Canadian Society for Chemical Engineering | *For Our Future*
Société canadienne de génie chimique | *Pour notre avenir*

A theoretical study of the reverse water-gas shift reaction on Ni(111) and Ni(311) surfaces

Min Zhang[1,2] | Bart Zijlstra[2] | Ivo A. W. Filot[2] | Fang Li[1] | Haiou Wang[1] | Jingde Li[1] | Emiel J. M. Hensen[2]

[1]Hebei Provincial Key Laboratory of Green Chemical Technology and High Efficient Energy Saving, School of Chemical Engineering and Technology, Hebei University of Technology, Tianjin, China

[2]Laboratory of Inorganic Materials and Catalysis, Schuit Institute of Catalysis, Department of Chemical Engineering and Chemistry, Eindhoven University of Technology, Eindhoven, The Netherlands

Correspondence
Jingde Li, Hebei Provincial Key Laboratory of Green Chemical Technology and High Efficient Energy Saving, School of Chemical Engineering and Technology, Hebei University of Technology, Tianjin 300130, China.
Email: jingdeli@hebut.edu.cn
Emiel J. M. Hensen, Laboratory of Inorganic Materials and Catalysis, Department of Chemical Engineering and Chemistry, Eindhoven University of Technology, PO Box 513, 5600 Manitoba, Eindhoven, The Netherlands.
Email: e.j.m.hensen@tue.nl

Funding information
National Natural Science Foundation of China, Grant/Award Number: 21776057; Natural Science Foundation of Hebei Province, Grant/Award Number: B2017202182; Natural Science Foundation of Tianjin City, Grant/Award Number: 17JCYBJC20100;18JCYBJC21500

Abstract

This paper presents a systematic comparison study of the surface redox reaction mechanism for reverse water-gas shift (RWGS) over Ni(111) and Ni(311) surfaces. Specifically, the most stable surface intermediates and the reaction kinetics involved in the direct CO_2 activation and water formation steps are computed with density functional theory calculations and compared for the two different Ni surfaces. The results show that CO_2, CO, O, H, OH, and H_2O species adsorb stronger on Ni(311) than on Ni(111). Compared to Ni(111), the overall barriers for direct CO_2 activation and water formation on Ni(311) are lower by 23 and 17 kJ/mol, respectively. These observations indicate that the RWGS reaction through the surface redox mechanism should be preferred on Ni(311).

KEYWORDS

carbon dioxide, DFT, nickel, reverse water-gas shift, surface redox

1 | INTRODUCTION

Due to its potential impact on climate change, CO_2 emissions from burning fossil fuels (coal, natural gas, and oil) have raised global concern. Fossil fuels are non-renewable sources of energy that will eventually deplete. Therefore, a significant amount of attention is geared towards concentrating and utilizing CO_2 as a feedstock for conversion into storage chemicals and chemical intermediates such as syngas, methane, methanol, formic acid, and ethylene.[1–8] Among various

CO_2 conversion approaches, the reduction of CO_2 with H_2 into CO and H_2O, which is known as the reverse water-gas shift (RWGS) reaction, has been considered a critical reaction. For example, the RWGS reaction is part of the kinetic network in the Sabatier reaction for methane production, methanol production, and the Fischer-Tropsch (FT) synthesis of liquid hydrocarbons.[9] The endothermic RWGS reaction requires a catalyst that can be operated at a relatively high temperature. Noble metal catalysts such as Pt, Rh, and Au usually have high activity and stability for the RWGS reaction[10–19]; however, their high cost limits their industrial application. Ni is a commonly used low-cost transition metal catalyst for the RWGS reaction.[20]

Many studies in the literature focus on the elucidation of the kinetic mechanism. Usually, it is assumed that during the reaction carboxyl (HOCO), formate (HCOO), carbonate (CO_3^{2-}), and bicarbonate (HCO_3^-) intermediates are formed on the Ni surface. Through a combined experimental and theoretical study, Vesselli et al[21] reported that on the Ni(110) surface HOCO is formed as an intermediate that is subsequently hydrogenated to formic acid (HCOOH).[21] Finally, a HCOO intermediate is generated. This result is in line with the work of Vogt et al,[22] who showed that surface CO_3^{2-} can be generated first, followed by the formation of a HCOO intermediate during the RWGS reaction over Ni/SiO_2 catalysts. In a study reported by Miyao et al,[23] CO_3^{2-} and HCO_3^- species were detected in the RWGS reaction using a Ni-Al-based catalyst.

In addition to these experimental studies, there are many theoretical investigations on Ni catalysts used in the RWGS reaction.[24–26] Two different RWGS reaction mechanisms have been proposed: (a) the HOCO pathway, in which CO_2 hydrogenation occurs prior to C—O bond scission to form CO and OH, and (b) the surface redox mechanism, involving direct CO_2 activation (C—O bond scission) and subsequent H_2O formation by the hydrogenation of the resulting O atom. Moreover, it has been reported that the preferred RWGS pathway depends on the type of metal and the surface termination. Dietz et al[24] performed a systematic density functional theory (DFT) study of RWGS reaction pathways on the planar (111) surface of Pt, Rh, Ni, Cu, Ag, and Pd metals. It was found that the RWGS reaction through the HOCO route is favoured on Pt, Ag, and Pd catalysts, whereas the surface redox mechanism is preferred over Rh, Ni, and Cu catalysts. A DFT study by Fan et al[25] showed that on Ni(111), Ni(211), and Ni(100), the RWGS reaction prefers to follow the surface redox mechanism over the HOCO pathway. Moreover, Lin et al[26] reported that, on Ni(110), the surface redox mechanism is preferred over the HOCO pathway. It has also been mentioned that both mechanisms benefit from subsurface hydrogen species. The above-reported DFT results suggest that on most Ni facets the HOCO pathway is less favourable than the surface redox mechanism. Accordingly, we focus in this study on the surface redox mechanism.

Stepped surfaces have attracted widespread attention because they were found to be essential in many catalytic processes involving metal nanoparticles.[27–35] Recently, a Ni(311) surface, which represents the step-edge interface of (111) and (100) nanofacets,[36] was found to play an important role in different surfaces reactions. For example, Liu et al[35] reported that Ni(311) presented the lowest barrier for CO activation among different Ni facets. Although there are many experimental and theoretical studies on the surface redox mechanism of the RWGS reaction over low-index Ni surfaces, the energetics of the surface redox mechanism over the Ni(311) surface have not yet been studied. Therefore, we explored this surface redox mechanism on Ni(311) step edges by determining relevant activation barriers in comparison to the planar Ni(111) surface. To the best of our knowledge, this is the first time that the surface redox pathway of the RWGS reaction is investigated by DFT on the Ni(311) surface. We present reaction energy diagrams (RED) for the RWGS reaction to compare the operating mechanism for Ni(311) and Ni(111) surfaces. The results may provide useful information for further studies on CO_2 hydrogenation over Ni-based catalysts.

2 | COMPUTATIONAL METHODS

All DFT calculations were done using the Vienna ab initio simulation package (VASP) using the Perdew-Burke-Ernzerhof exchange-correlation functional.[37–40] The valence electrons were modelled using a plane-wave basis set with a cut-off energy of 400 eV (1 eV ≈ 96 kJ/mol). The projector augmented-wave (PAW) method was used to model the core electrons.[41,42] The Brillouin zone was sampled using a Monkhorst-Pack mesh of *k*-points with a $2 \times 2 \times 1$ grid for the species in the gas phase and a $3 \times 3 \times 1$ and $3 \times 6 \times 1$ grid for the Ni(111) and Ni(311) slab surfaces, respectively.[43] The *k*-points selection is based on that the sampling density in the reciprocal space is approximately similar on both surfaces. According to our *k*-point optimization, the differences in CO_2 adsorption energies on Ni(111) and Ni(311) are <5 kJ/mol when the *k*-point grid is refined to $4 \times 4 \times 1$ and $4 \times 7 \times 1$ for Ni(111) and Ni(311), respectively. The Gaussian smearing of the partial occupancies for each wave function was set to a width of 0.05 eV. The adsorbate was placed at the centre of a $1 \times 1 \times 1$ nm^3 unit cell for the gas-phase calculations. We have used a Monkhorst-Pack *k*-point grid of $10 \times 10 \times 10$ for the Ni crystal. The optimized bulk lattice constant for Ni was found to be 0.353 nm, which is in good agreement with the experimental value of 0.352 nm.[44] To avoid the spurious interaction of neighbouring super cells, a vacuum height of 1.5 nm in the direction parallel for the crystal surface was employed.

The Ni(111) and Ni(311) surfaces are modelled using a (4×4) and (2×2) unit cell with three and eight atomic layers, respectively. The bottom two and four layers were frozen at their bulk positions for Ni(111) and Ni(311), respectively. The remaining Ni layers and surface adsorbates were allowed to relax until the forces were <0.2 eV/nm. The optimized Ni(111) and Ni(311) surfaces are shown in Figure 1. Herein, it can be seen that the Ni(111) surface has top, bridge, hcp, and fcc sites, whereas the Ni(311) surface contains top, bridge, 4-fold, hcp, and fcc sites.

The climbing-image nudged elastic band (CI-NEB) approach and the improved force reversed method were employed to search for the transition state (TS).[45–47] A frequency analysis was performed to verify that each transition state corresponds to a first-order saddle point on the potential energy surface with a single imaginary frequency in the direction of the reaction coordinate. Herein, the frequencies were sampled by the construction of a Hessian matrix based on a finite difference approach wherein the atomic positions were perturbed in all Cartesian directions by 0.002 nm. The reaction barriers were obtained by considering $E_f = E_{TS} - E_{reactants}$, where E_{TS} represents the energy of the transition state. The adsorption energy of surface species was defined as $E_{ads} = E_{(slab + adsorbate)} - E_{(slab)} - E_{(adsorbate)}$, where the $E_{slab + adsorbate}$ represents the total energies of the optimized adsorbate on the surface, E_{slab} is the energy of the slab, and $E_{adsorbate}$ stands for the energy of the adsorbate in the gas phase. A more negative value of the adsorption energy represents a stronger interaction between the adsorbates and the surface. In a similar fashion, a negative value of the reaction energy indicates that the reaction is exothermic, whereas a positive value implies that it is an endothermic reaction.

The Gibbs free energy of adsorption, ΔG, is given by the following equation:

$$\Delta G = \Delta H - T\Delta S \quad (1)$$

where ΔH is the enthalpic change from the gas-phase state to the adsorbed state (ie, the adsorption energy) and $T\Delta S$ denotes the entropy contribution from the change of entropy (ΔS) at temperature T.

A molecule made of N atoms has in total $3N$ degrees of freedom. A linear molecule has $3N - 5$ vibrational, three translational and two rotational degrees of freedom in the gas-phase state. In contrast, a nonlinear molecule in the gas phase has $3N-6$ vibrational, three translational and three rotational degrees of freedom. The transitional and rotational degrees of freedom will be replaced by the vibrational degrees of freedom for the adsorbed molecule on the surface. Therefore, there are $3N$ vibrational modes in the adsorbed state. The entropy of the transition state has $3N-1$ vibrational modes. The vibrational entropy contribution to the free energy of association is given by the following:

$$TS_{vib} = \sum_{i=1}^{3N} \left(\frac{h\nu_i}{e^{\frac{h\nu_i}{k_B T}} - 1} - \frac{h\nu_i}{2} - k_B T \ln\left(1 - e^{-\frac{h\nu_i}{k_B T}}\right) \right) \quad (2)$$

where k_B is the Boltzmann constant; h is the Planck constant; and ν_i is the vibrational frequency for the ith normal mode.

3 | RESULTS AND DISCUSSION

3.1 | Adsorbate stability on Ni(111) and Ni(311) surfaces

The most stable adsorption configurations and the corresponding adsorption energies of the surface species involved in the RWGS reaction on Ni(111) and Ni(311) surfaces are shown in Figure 2. From this figure, it can be clearly seen that the CO_2 adsorption is

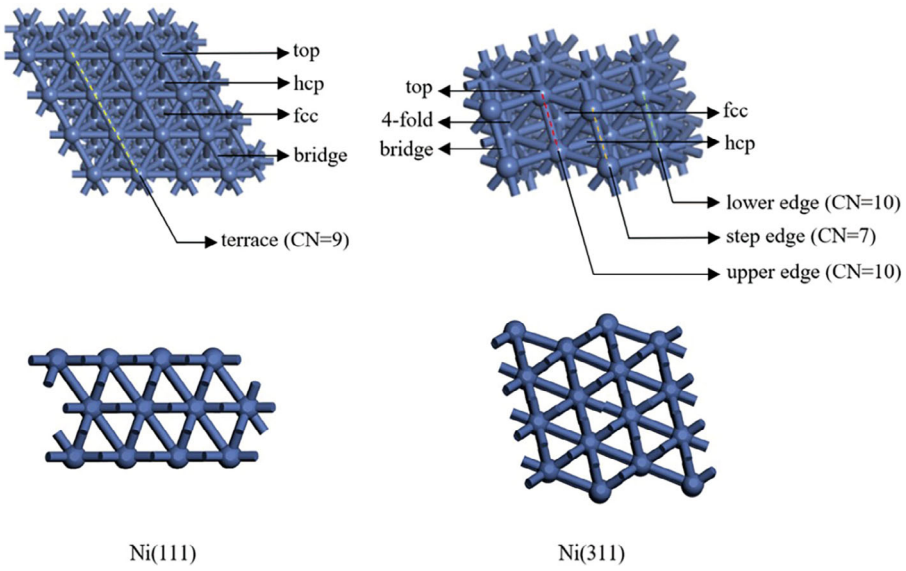

FIGURE 1 Top view and side view of the optimized Ni(111) surface (left) and Ni(311) surface (right). Important adsorption sites have been highlighted. The coordination numbers (CN) for the surface atoms of each row are labelled

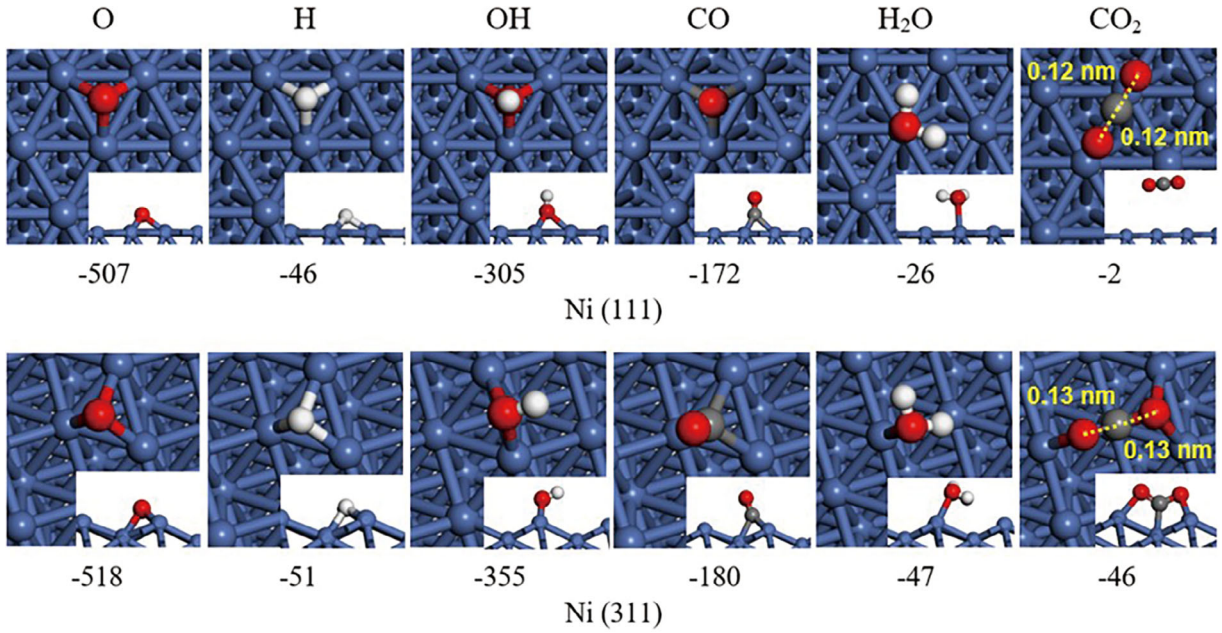

FIGURE 2 Top view and side view (inset) of the most stable configurations and the corresponding adsorption energies (kJ/mol) of the adsorbates involved in the RWGS reaction on the Ni(111) surface (top) and the Ni(311) surface (bottom). Blue, gray, red, and white spheres represent Ni, C, O, and H atoms, respectively

significantly stronger on the Ni(311) surface. This result is expected from the bond order conservation principle as the coordination number of the surface atoms in Ni(111) is nine, while the Ni(311) surface contains a surface atom with a coordination number of seven (Figure 1).[48]

For the atomic species (ie, O and H), it can be seen that the preferred adsorption mode is similar for the Ni(111) and Ni(311) surfaces. The O atom prefers to occupy the 3-fold site on both Ni(111) (E_{ads} = −507 kJ/mol) and Ni(311) (E_{ads} = −518 kJ/mol). A similar result is found for H, which also has a preferential 3-fold adsorption mode with energy differences of −46 and − 51 kJ/mol on the Ni(111) and Ni(311) surfaces, respectively, with respect to the gas phase. For the hydroxyl moiety (OH), the preferred adsorption mode is the fcc site on Ni(111) with E_{ads} = −305 kJ/mol. In contrast, OH adsorbs much stronger, by 50 kJ/mol, on the Ni(311) in a bridge mode. The CO molecule prefers to adsorb in a 3-fold coordination mode on Ni(111) and Ni(311) with comparable respective adsorption energies of −172 and − 180 kJ/mol. Again, these results are in agreement with previous DFT calculations.[35,49] H_2O binds weakly on a top site on both Ni(111) and Ni(311) with adsorption energies of −26 and − 47 kJ/mol, respectively. Herein, the Ni-O bond length between the Ni atom and the O atom of adsorbed H_2O molecule is 0.22 nm for the Ni(111) surface, which is in good agreement with previous results from the literature.[50] In comparison, the Ni-O bond length for the Ni(311) is 0.21 nm, consistent with the stronger adsorption. Interestingly, whereas CO_2 can only be physisorbed on the flat Ni(111) surface with an adsorption energy of −2 kJ/mol, in line with previous findings,[49,51] it was found to strongly adsorb in a bidentate fashion on the Ni(311) surface with an adsorption energy of −46 kJ/mol. From the C—O bond lengths (0.13 nm) in CO_2, it can be seen that the CO_2 molecule is already pre-activated upon adsorption on the Ni(311) surface, whereas the C—O bond lengths are both 0.12 nm for adsorption on Ni(111), almost unchanged with regard to the gas-phase values.

3.2 | CO_2 activation

In Figure 3, the initial, transition, and final states for direct CO_2 dissociation are depicted. The corresponding barriers are given in Table 1. By using CI-NEB calculations, we identified a two-step direct CO_2 dissociation pathway over Ni(111): initially, physisorbed CO_2 migrates towards the surface to form a metastable state wherein one of the oxygen atoms of CO_2 is bound to a top site (Figure 3A). This metastable state is 25 kJ/mol less stable than physisorbed CO_2 on Ni(111). The C—O bond lengths of this metastable state are 0.13 and 0.12 nm, indicating that this state leads to activation of the CO molecule. The reaction barrier from physisorbed CO_2 to the metastable state is 39 kJ/mol. The C—O bond lengths at the TS_1 are both 0.12 nm. The second step is the dissociation of the metastable state into CO and O, which has an activation barrier of 49 kJ/mol and is exothermic by 95 kJ/mol. In the TS_2, the CO molecule migrates over a Ni atom towards a 3-fold site, whereas the O

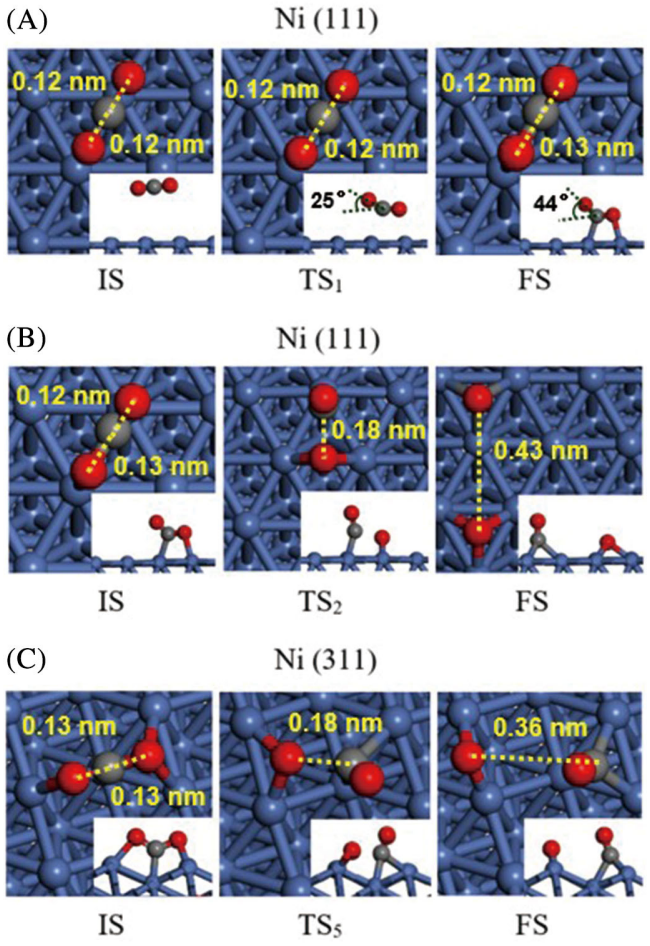

FIGURE 3 Top view and side view (inset) of initial state (IS), transition state (TS), and final state (FS) involved in the direct CO_2 dissociation on the Ni(111) surface (top and middle) and the Ni(311) surface (bottom). Blue, gray, and red spheres represent Ni, C, and O atoms, respectively

TABLE 1 The forward (E_f) and backward (E_b) activation energies (kJ/mol) for the direct CO_2 activation on the Ni(111) and Ni(311) surfaces

	Ni(111)		Ni(311)	
Reaction	**E_f**	**E_b**	**E_f**	**E_b**
$CO_2{}^*{}_{phys} > CO_2{}^*$	39	14	…	…
$CO_2{}^* + * > CO^* + O^*$	49	144	78	123

atom migrates to a 3-fold site via a bridge site. The C—O bond distance of the dissociating O atom is 0.18 nm in the TS_2. The two-step CO_2 dissociation reaction has, thus, an overall activation energy of 74 kJ/mol and is exothermic by 70 kJ/mol.

Direct CO_2 dissociation over Ni(311) proceeds in a single step. It has a reaction barrier of 78 kJ/mol and a reaction energy of −45 kJ/mol. We choose CO_2 adsorbed in its most stable adsorption mode as the initial state (IS). In the TS_5, the CO moves to the 3-fold coordinated site through the bridge site on the terrace, while the O atom migrates to the neighbouring bridge site. The C—O bond distance is increased to 0.18 nm. Finally, in the final state (FS) the CO molecule is adsorbed at the 3-fold site and the O atom is bound to the bridge site at the step edge. The distance between CO and atomic O in the FS is 0.36 nm.

Furthermore, we studied the energetics of the HOCO pathway on Ni(311). As the first reaction step, ie, CO_2 hydrogenation to the HOCO intermediate, is usually considered as the rate-determining step in the HOCO pathway,[25,26] only the energy barrier of CO_2 hydrogenation reaction was calculated. It was found that this reaction step has an energy barrier of 132 kJ/mol, which is much higher than that of direct CO_2 activation on Ni(311) (78 kJ/mol). Therefore, our assumption to focus on the surface redox mechanism on Ni(311) and Ni(111) surfaces is warranted.

3.3 | H_2O formation

The resulting oxygen of the CO_2 dissociation can be removed from the surface as H_2O by two-step hydrogenation of the O atom. The corresponding IS, TS, and FS configurations for the formation of OH and H_2O are shown in Figures 4 and 5, respectively. The corresponding reaction energies are listed in Table 2. From this Table, it can be seen that O hydrogenation towards OH over Ni(111) has an activation energy of 106 kJ/mol and is mildly endothermic by 11 kJ/mol. Initially, the O and H atoms are adsorbed in a 3-fold coordination and separated by 0.27 nm. In the TS_3, the hydrogen atom moves towards the adsorbed oxygen species by which the O—H bond length is decreased to 0.14 nm. In the final state, hydroxyl is formed and is adsorbed in a 3-fold coordination with an O—H bond length of 0.10 nm. These values agree with the previous results.[52] Subsequently, the hydroxyl species can be further hydrogenated to form surface H_2O. This reaction has a barrier of 117 kJ/mol and is endothermic by 25 kJ/mol. In the IS, both the OH molecule and H atom are adsorbed in two adjacent fcc sites wherein a single metal atom is shared. In the TS_4, both the OH molecule and the H atom move towards the shared metal atom. Herein, the corresponding O—H bond is shortened to 0.16 nm. In the FS, the H_2O molecule is adsorbed on a top site.

For the Ni(311) model, the formation of OH has a lower activation energy (81 kJ/mol) with respect to the Ni(111) surface (106 kJ/mol). The corresponding reaction energy is −22 kJ/mol. In the IS, the O atom is located at the bridge site and the H atom at the fcc site. The O—H bond length in TS_6 is 0.15 nm. The FS includes the OH species at the bridge site. Subsequently, the OH species can be hydrogenated to

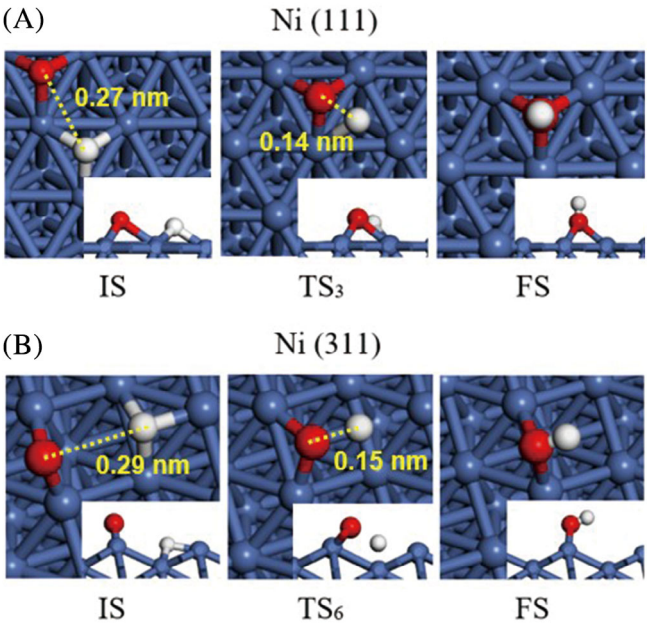

FIGURE 4 Top view and side view (inset) of the optimized structures of IS, TS, and FS in the OH formation on the Ni(111) surface (top) and the Ni(311) surface (bottom). Blue, white, and red spheres represent Ni, H, and O atoms, respectively

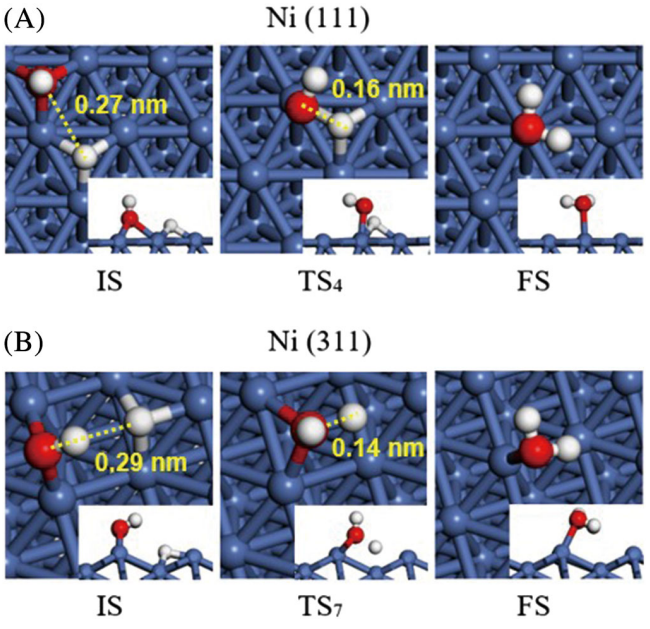

FIGURE 5 Top view and side view (inset) of optimized configurations of IS, TS, and FS in the H_2O formation on the Ni(111) surface (top) and the Ni(311) surface (bottom). Blue, white, and red spheres represent Ni, H, and O atoms, respectively

yield adsorbed H_2O. This process is endothermic by 58 kJ/mol and has a reaction barrier of 111 kJ/mol. For the IS, we selected a co-adsorption state with the H occupying a 3-fold site and the OH staying in the bridge site. In the TS_7, the OH molecule is bound to the bridge site by slightly migrating to the quasi-4-fold coordination, whereas the H atom moves towards the O atom of OH. The corresponding O─H bond length is reduced to 0.14 nm. The FS involves the H_2O molecule at the top site.

TABLE 2 The forward (E_f) and backward (E_b) activation energies (kJ/mol) for the H_2O formation on the Ni(111) and Ni(311) surfaces

	Ni(111)		Ni(311)	
Reaction	**E_f**	**E_b**	**E_f**	**E_b**
O* + H* > OH* + *	106	95	81	103
OH* + H* > H_2O* + *	117	92	111	53

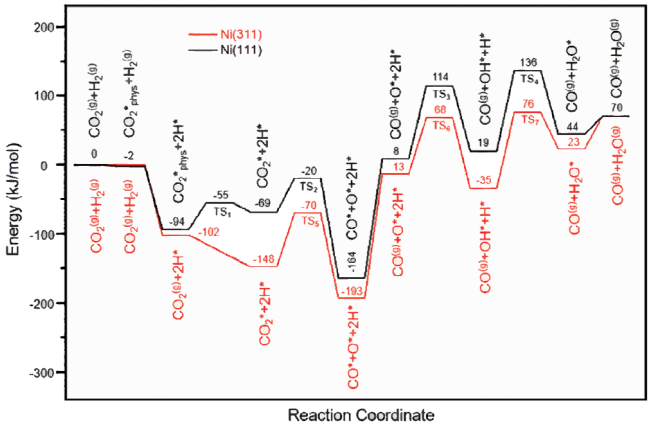

FIGURE 6 Reaction energy diagram of the RWGS reaction on the Ni(111) and Ni(311) surfaces. All values are labelled in kJ/mol

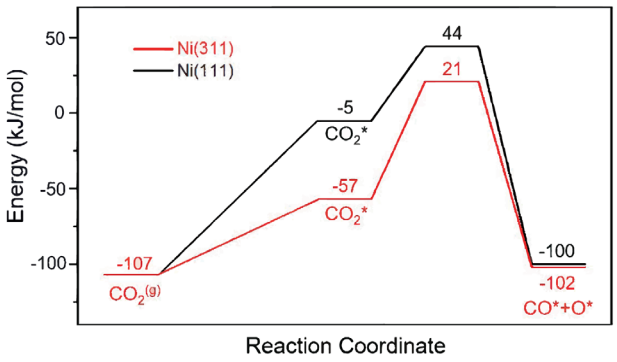

FIGURE 7 Gibbs free energy diagram of CO_2 dissociation on the Ni(111) and Ni(311) surfaces at 500 K. All values are labelled in kJ/mol

3.4 | Reaction energy diagram

In Figure 6, the RED for the RWGS reaction over Ni(111) and Ni(311) is given. From this Figure, it can be seen that the barrier of direct CO_2 activation over Ni(111) is 74 kJ/mol, similar to the barrier of 78 kJ/mol over Ni(311). In a

Surface	ν_i (cm^{-1})								
Ni(111)	1745.7	1116.6	637.3	482.9	278.8	163.3	123.1	80.4	12.0
Ni(311)	1458.4	1100.2	701.8	431.8	328.0	283.9	189.1	169.8	81.0

TABLE 3 Vibrational frequencies (ν_i) of metastable CO_2 on Ni(111) and adsorbed CO_2 on Ni(311)

previous DFT study by Fan et al,[25] it was found that the planar Ni(111) surface and the stepped Ni(211) surface have similar barriers for direct CO_2 activation (65 vs 71 kJ/mol). This suggests that the stepped Ni(311) surface exhibits a similar catalytic activity with the Ni(211) surface towards direct CO_2 activation. Furthermore, their work revealed that compared with Ni(111) and Ni(211), the open Ni(100) surface has the lowest barrier (35 kJ/mol) for direct CO_2 activation.

Although the enthalpic barriers of direct CO_2 activation on Ni(111) and Ni(311) are similar, the effect of entropy on the energetics is significant. This can be further demonstrated in the Gibbs free energy diagram, as shown in Figure 7. In the analysis of Gibbs free energy, the temperature in Equations (1) and (2) was set at 500 K as a representative reaction temperature. At 500 K, the contribution of the entropic term of the CO_2 molecule to the Gibbs free energy is 107 kJ/mol. Based on Equation (2) and the frequency data of CO_2 in Table 3, an entropic contribution of 11 kJ/mol is associated with the vibrational degrees of freedom of adsorbed CO_2 on Ni(311), indicating that 96 kJ/mol is lost during the adsorption step. According to Equation (1), the Gibbs free energy for CO_2 adsorption is 50 kJ/mol. Combining this value with the enthalpic CO_2 dissociation barrier results in an overall CO_2 dissociation barrier of 128 kJ/mol on Ni(311). In a similar manner, the vibrational entropy for adsorbed CO_2 in the metastable state (E_{ads} = +23 kJ/mol) on Ni(111) was calculated to be 28 kJ/mol, which indicates that the total entropy loss is 79 kJ/mol for CO_2 adsorption. Therefore, the Gibbs free energy for CO_2 adsorption is 102 kJ/mol, which leads to an overall CO_2 dissociation barrier of 151 kJ/mol on Ni(111). Obviously, these values will be affected by the accuracy of the parameters, for which a future sensitivity analysis in combination with microkinetic modelling would be most informative.[53–56]

The rate of CO_2 desorption is expected to be much higher than that of C—O bond dissociation on Ni(111). This is due to the weak adsorption of CO_2 over Ni(111) and will result in a very low coverage of adsorbed CO_2. For Ni(311), we expect a low coverage as well, although CO_2 adsorbs stronger by 44 kJ/mol and the overall Gibbs free energy for CO_2 dissociation is 23 kJ/mol lower than on Ni(111). Therefore, it is clear that the overall rate of CO_2 activation will be significantly higher on Ni(311) than on Ni(111). The RED also shows that H_2O formation from the subsequent oxygen hydrogenation has an overall activation barrier of 128 kJ/mol on Ni(111) and 111 kJ/mol on Ni(311). Therefore, H_2O formation is also preferred on Ni(311). These findings indicate that CO_2 dissociation will preferentially occur on the stepped Ni(311) surface and CO_2 adsorption, CO_2 dissociation, and H_2O formation will be potential rate-controlling steps.

The surface energy of Ni(311) was calculated to be 14 300 meV/nm^2 (1 meV = 1.6×10^{-13} J), which is much lower than that of Ni(10$\bar{1}$0)B surface (16 000 meV/nm^2).[35] The latter has the highest surface energy among all Ni facets. Therefore, it may be expected that the Ni(311) configuration appears at the surface of the metal nanoparticles. In the literature, various methods have been developed to expose (311) facets under appropriate conditions.[57,58] For example, Wang et al[57] developed a cation exchanging reaction to synthesize FePt nano-dendrites with large surface areas and exposure of (311) facets. Find et al[58] revealed that anisotropic recrystallization of Pt black favoured the exposure of (220) and (311) planes under hydrogen-induced conditions. Furthermore, the doubling of step heights of a single crystal when heating it in hydrogen can preferentially expose (311) facets. Therefore, these methods might be applied in preparing Ni catalysts to preferentially expose (311) facets to promote the catalytic activity of the RWGS reaction.

4 | CONCLUSIONS

In this work, the energetics of the RWGS reaction on Ni(111) and Ni(311) surfaces following the surface redox mechanism were systematically investigated using DFT. CO_2, CO, O, H, OH, and H_2O surface species adsorb stronger on Ni(311) than on Ni(111). The overall barrier for C—O bond breaking in CO_2 activation on Ni(111) is higher by 23 kJ/mol than the barrier found on Ni(311). H_2O formation on Ni(311) has an activation energy of 111 kJ/mol, which is lower by 17 kJ/mol than the overall barrier on Ni(111). By comparing the reaction pathways of the RWGS reaction on the two Ni facets, it is suggested that Ni(311) is more active than Ni(111) for the surface redox mechanism.

ACKNOWLEDGEMENTS

This work was carried out on the Dutch national e-infrastructure with the support of the Netherlands Organization for Scientific Research (NWO). We acknowledge financial

support from the National Natural Science Foundation of China (No. 21776057), Natural Science Foundation of Tianjin (No. 17JCYBJC20100, No. 18JCYBJC21500), and Natural Science Foundation of Hebei Province (No. B2017202182).

REFERENCES

[1] H. Arandiyan, Y. Wang, J. Scott, S. Mesgari, H. Dai, R. Amal, *ACS Appl. Mater. Inter.* **2018**, *10*, 16352.
[2] K. Larmier, W. C. Liao, S. Tada, E. Lam, R. Verel, A. Bansode, A. Urakawa, A. Comas-Vives, C. Copéret, *Angew. Chem. Int. Edit.* **2017**, *56*, 2318.
[3] J. M. Saveant, C. Tard, *J. Am. Chem. Soc.* **2016**, *138*, 1017.
[4] K. Rohmann, J. Kothe, M. W. Haenel, U. Englert, M. Hölscher, W. Leitner, *Angew. Chem. Int. Edit.* **2016**, *55*, 8966.
[5] A. Álvarez, A. Bansode, A. Urakawa, A. V. Bavykina, T. A. Wezendonk, M. Makkee, J. Gascon, F. Kapteijn, *Chem. Rev.* **2017**, *117*, 9804.
[6] Q. Zhu, J. Ma, X. Kang, X. Sun, H. Liu, J. Hu, Z. Liu, B. Han, *Angew. Chem.* **2016**, *128*, 9158.
[7] K. D. Yang, W. R. Ko, J. H. Lee, S. J. Kim, H. Lee, M. H. Lee, K. T. Nam, *Angew. Chem. Int. Edit.* **2017**, *56*, 796.
[8] D. A. Torelli, S. A. Francis, J. C. Crompton, A. Javier, J. R. Thompson, B. S. Brunschwig, M. P. Soriaga, N. S. Lewis, *ACS Catal.* **2016**, *6*, 2100.
[9] F. Fischer, H. Tropsch, *Brennst. Chem.* **1923**, *4*, 276.
[10] I. Ro, C. Sener, T. M. Stadelman, M. R. Ball, J. M. Venegas, S. P. Burt, I. Hermans, J. A. Dumesic, G. W. Huber, *J. Catal.* **2016**, *344*, 784.
[11] S. Kattel, B. Yan, J. G. Chen, P. Liu, *J. Catal.* **2016**, *343*, 115.
[12] B. Liang, H. Duan, X. Su, X. Chen, Y. Huang, X. Chen, J. J. Delgado, T. Zhang, *Catal. Today* **2017**, *281*, 319.
[13] X. Chen, X. Su, B. Liang, X. Yang, X. Ren, H. Duan, Y. Huang, T. Zhang, *J. Energy Chem.* **2016**, *25*, 1051.
[14] D. Tibiletti, A. Goguet, F. C. Meunier, J. P. Breen, R. Burch, *Chem. Commun.* **2004**, **10**, 1636.
[15] F. Samimi, N. Hamedi, M. R. Rahimpour, *J. Environ. Chem. Eng.* **2019**, *7*, 102813.
[16] F. V. Vázquez, P. Pfeifer, J. Lehtonen, P. Piermartini, P. Simell, V. Alopaeus, *Ind. Eng. Chem. Res.* **2017**, *56*, 13262.
[17] I. Ro, R. Carrasquillo-Flores, J. A. Dumesic, G. W. Huber, *Appl. Catal. A-Gen.* **2016**, *521*, 182.
[18] A. A. Upadhye, I. Ro, X. Zeng, H. J. Kim, I. Tejedor, M. A. Anderson, J. A. Dumesic, G. W. Huber, *Catal. Sci. Technol.* **2015**, *5*, 2590.
[19] L. C. Wang, D. Widmann, R. J. Behm, *Catal. Sci. Technol.* **2015**, *5*, 925.
[20] J. Liu, C. Li, F. Wang, S. He, H. Chen, Y. Zhao, M. Wei, D. G. Evans, X. Duan, *Catal. Sci. Technol.* **2013**, *3*, 2627.
[21] E. Vesselli, M. Rizzi, L. D. Rogatis, X. Ding, A. Baraldi, G. Comelli, L. Savio, L. Vattuone, M. Rocca, P. Fornasiero, A. Baldereschi, M. Peressi, *J. Phys. Chem. Lett.* **2010**, *1*, 402.
[22] C. Vogt, E. Groeneveld, G. Kamsma, M. Nachtegaal, L. Lu, C. J. Kiely, P. H. Berben, F. Meirer, B. M. Weckhuysen, *Nat. Catal.* **2018**, *1*, 127.
[23] T. Miyao, W. Shen, A. Chen, K. Higashiyama, M. Watanabe, *Appl. Catal. A-Gen.* **2014**, *486*, 187.
[24] L. Dietz, S. Piccinin, M. Maestri, *J. Phys. Chem. C* **2015**, *119*, 4959.
[25] C. Fan, Y. A. Zhu, M. L. Yang, Z. J. Sui, X. G. Zhou, D. Chen, *Ind. Eng. Chem. Res.* **2015**, *54*, 5901.
[26] W. Lin, K. M. Stocker, G. C. Schatz, *J. Phys. Chem. C* **2016**, *120*, 23061.
[27] J. Li, E. Croiset, L. Ricardez-Sandoval, *J. Mol. Catal. A-Chem.* **2012**, *365*, 103.
[28] I. A. W. Filot, R. A. van Santen, E. J. M. Hensen, *Angew. Chem. Int. Edit.* **2014**, *53*, 12746.
[29] I. A. W. Filot, R. A. van Santen, E. J. M. Hensen, *Catal. Sci. Technol.* **2014**, *4*, 3129.
[30] B. Zijlstra, R. J. P. Broos, W. Chen, I. A. W. Filot, E. J. M. Hensen, *Catal. Today* **2019**. https://doi.org/10.1016/j.cattod.2019.03.002.
[31] I. A. W. Filot, S. G. Shetty, E. J. M. Hensen, R. A. van Santen, *J. Phys. Chem. C* **2011**, *115*, 14204.
[32] J. X. Liu, H. Y. Su, D. P. Sun, B. Y. Zhang, W. X. Li, *J. Am. Chem. Soc.* **2013**, *135*, 16284.
[33] J. X. Liu, H. Y. Su, W. X. Li, *Catal. Today* **2013**, *215*, 36.
[34] R. A. Van Santen, A. J. Markvoort, I. A. W. Filot, M. M. Ghouri, E. J. M. Hensen, *Phys. Chem. Chem. Phys.* **2013**, *15*, 17038.
[35] J. X. Liu, B. Y. Zhang, P. P. Chen, H. Y. Su, W. X. Li, *J. Phys. Chem. C* **2016**, *120*, 24895.
[36] P. Schilbe, S. Siebentritt, K.-H. Rieder, *Chem. Phys. Lett.* **1995**, *233*, 569.
[37] G. Kresse, J. Hafner, *Phys. Rev. B* **1993**, *47*, 558.
[38] G. Kresse, J. Furthmuller, *Phys. Rev. B* **1996**, *54*, 11169.
[39] G. Kresse, J. Furthmuller, *Comput. Mater. Sci.* **1996**, *6*, 15.
[40] J. P. Perdew, K. Burke, M. Ernzerhof, *Phys. Rev. Lett.* **1996**, *77*, 3865.
[41] P. Blochl, *Phys. Rev. B* **1994**, *50*, 17953.
[42] G. Kresse, D. Joubert, *Phys. Rev. B* **1999**, *59*, 1758.
[43] H. J. Monkhorst, J. D. Pack, *Phys. Rev. B* **1976**, *13*, 5188.
[44] A. Taylor, *J. I. Met.* **1950**, *77*, 585.
[45] G. Henkelman, B. P. Uberuaga, H. Jónsson, *J. Chem. Phys.* **2000**, *113*, 9901.
[46] G. Henkelman, H. Jónsson, *J. Chem. Phys.* **2000**, *113*, 9978.
[47] K. J. Sun, Y. H. Zhao, H. Y. Su, W. X. Li, *Theor. Chem. Acc.* **2012**, *131*, 11181.
[48] E. Shustorovich, *Surf. Sci. Rep.* **1986**, *6*, 1.
[49] Y. A. Zhu, D. Chen, X. G. Zhou, W. K. Yuan, *Catal. Today* **2009**, *148*, 260.
[50] A. A. Phatak, W. N. Delgass, F. H. Ribeiro, W. F. Schneider, *J. Phys. Chem. C* **2009**, *113*, 7269.
[51] G. Peng, S. J. Sibener, G. C. Schatz, S. T. Ceyer, M. Mavrikakis, *J. Phys. Chem. C* **2012**, *116*, 3001.
[52] J. Ren, H. Guo, J. Yang, Z. Qin, J. Lin, Z. Li, *Appl. Surf. Sci.* **2015**, *351*, 504.
[53] L. A. Ricardez-Sandoval, *Can. J. Chem. Eng.* **2011**, *89*, 1324.
[54] S. Rasoulian, L. A. Ricardez-Sandoval, *Chem. Eng. Sci.* **2014**, *116*, 590.

[55] D. Chaffart, S. Rasoulian, L. A. Ricardez-Sandoval, *AIChE J.* **2016**, *62*, 2374.

[56] D. Chaffart, L. A. Ricardez-Sandoval, *Comput. Chem. Eng.* **2018**, *119*, 465.

[57] D. Y. Wang, H. L. Chou, C. C. Cheng, Y. H. Wu, C. M. Tsai, H. Y. Lin, Y. L. Wang, B. J. Hwang, C. C. Chen, *Nano Energy* **2015**, *11*, 631.

[58] J. Find, Z. Paál, R. Schlögl, U. Wild, *Catal. Lett.* **2000**, *65*, 19.

How to cite this article: Zhang M, Zijlstra B, Filot IAW, et al. A theoretical study of the reverse water-gas shift reaction on Ni(111) and Ni(311) surfaces. *Can J Chem Eng*. 2020;98:740–748. https://doi.org/10.1002/cjce.23655